Optical pumping of high-density Rb with a broadband dye laser and GaAlAs diode laser arrays: Application to ³He polarization

M. E. Wagshul and T. E. Chupp

The Physics Laboratories, Harvard University, Cambridge, Massachusetts 02138 (Received 21 December 1988; revised manuscript received 11 July 1989)

We have studied laser optical pumping of Rb at densities up to 4×10^{14} atoms/cm³ and produced polarized ³He by spin exchange with Rb. Numerical calculations show that for a high-density Rb vapor GaAlAs diode laser arrays can provide results similar to those obtained with a broadband Kr⁺-ion-dye-laser system. We have confirmed these calculations with measurements using a 40-GHz full width at half maximum bandwidth dye laser and 100- and 500-mW GaAlAs diode laser arrays (Spectra Diode Labs Array Nos. SDL-2410C and SDL-2450C). We have optically pumped Rb of density [Rb]=4×10¹⁴ atoms/cm³, and we have measured up to 70% ³He polarization in a 4-cm³ volume with 600 mW from the dye laser. With the diode laser arrays, we have pumped with 30 and 300 mW with results comparable to those obtained with the dye laser. With a 1-W diode laser array, we anticipate 70-80 % ³He polarization in a 4-cm³ volume.

I. INTRODUCTION

Polarized, high-density ³He samples are being applied as polarized targets, as a neutron polarizer, and for magnetometry in precision frequency measurements.4 These samples are produced by spin exchange between the ³He and optically pumped Rb vapor. The Rb density necessary to produce ³He polarization of 50% or greater is $[Rb] \approx 4 \times 10^{14}$ atoms/cm³, which represents a previously unstudied regime of optical pumping of alkali-metal atoms. We have pursued studies⁵ begun with the successful polarization of ²¹Ne in order to optimize ³He polarization and explore the utility of alternative lasers such as GaAlAs diode laser arrays. (GaAlAs is the manufacturers's designation for these diode laser arrays.)

The technique of ³He polarization by spin exchange with optically pumped Rb was first demonstrated by Bouchiat, Carver, and Varnum. Gamblin and Carver continued the studies. In this early work, Rb was optically pumped by light from a discharge lamp, and the maximum Rb density was about 3×10^{12} atoms/cm³. Radiation trapping, the multiple scattering of unpolarized resonant light which depolarizes the Rb atoms, has also limited the Rb density. Consequently, the ³He polarizations obtained were much less than 1% since the rate of spin transfer from the Rb to the ³He is small compared to the 3 He spin-relaxation rates. Recently, lasers have been used, and for Rb densities up to 4×10^{14} atoms/cm 3 , radiation trapping has been shown to be suppressed with N₂. 1,5 Seventy percent polarization of 10²⁰ atoms/cm³ of ³He in a 4-cm³ volume has been demonstrated.³

Laser light for Rb optical pumping can be produced by broadband and single-mode dye lasers and by GaAlAs diode laser arrays. We have used a broadband dye laser (Coherent model CR-599) with a time averaged output spectrum well represented by a 40-GHz full width at half maximum (FWHM) Lorentzian. This laser has also been made to run as a narrow-band (≈3 GHz) laser with a single thin intracavity étalon. GaAlAs diode laser arrays have been produced with continuous wave (cw) power up to 1 W. However, the geometry of the gain-guided array is such that one element is not in phase with another. Consequently, the output has a spectrum such as that shown in Fig. 1. The 150-GHz separation of the peaks in Fig. 1 corresponds to the longitudinal-mode spacing of the 1000-\mu laser cavity. Techniques have been developed to narrow this output with optical feedback from an étalon⁸ as shown in Fig. 2 and by using the diode laser array as an amplifier for injected light. 9,10 These techniques are both quite effective, but not necessary for our application to polarizing ³He.

As we will demonstrate, in the regime of high-Rb density and buffer-gas pressure, laser light detuned by several hundred gigahertz from the Rb D1 resonance can

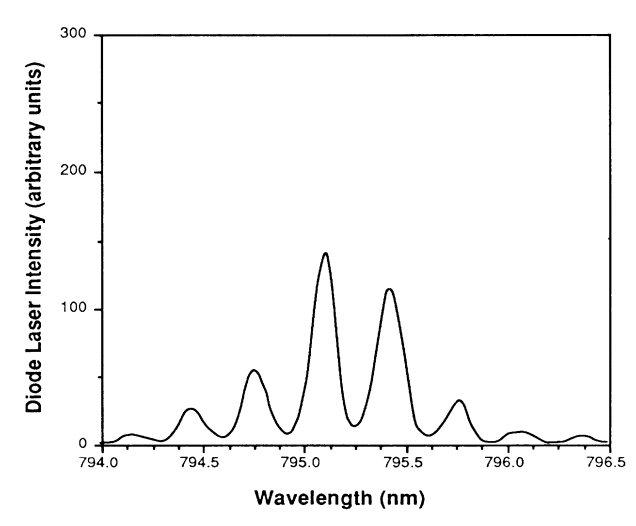


FIG. 1. Output spectrum of the SDL-2410C laser diode array cooled to 12.5 °C. The injection current is 400 mA. The array, as selected, emits near 797 nm at 20 °C. The mode spacing is 150 GHz.

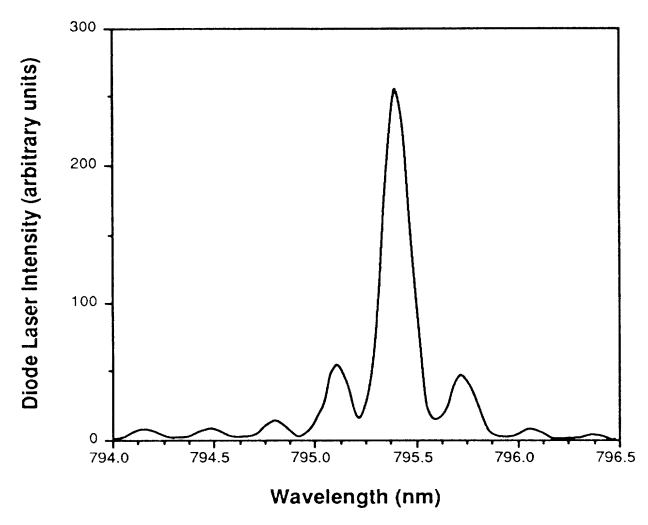


FIG. 2. Output spectrum of the SDL-2410C with optical feedback from a 50- μ m-thick, uncoated étalon as shown in the schematic.

effectively optically pump the vapor in cells in which the linewidth of the Rb D1 line is 15-65 GHz. Thus the entire broadband dye-laser spectrum and a large fraction of the GaAlAs diode laser array spectrum are useful.

In this paper we present the principles and results of numerical calculations of Rb polarization produced by optical pumping with a broadband (40-GHz linewidth) dye laser and with the diode laser array. These calculations are confirmed by measurements of Rb and ³He polarization produced with the dye laser and 100- and 500-mW diode laser arrays (Spectra Diode Labs SDL-2410C and SDL-2450C).

II. LASER OPTICAL PUMPING OF HIGH-DENSITY ALKALI-METAL VAPOR

The principle of optical pumping is illustrated in Fig. 3 for Rb for which $j = \frac{1}{2}$ in the ground state. In Fig. 3, the nuclear spin is neglected and the relevant states are the $5s_{1/2}$ state and the $5p_{1/2}$ state, each with two magnetic substates $m_s = \pm \frac{1}{2}$. The nuclear spin introduces hyperfine splitting of 3.036 GHz for 85 Rb (72.17% natural abundance) and 6.868 GHz for 87 Rb (27.83% natural abundance). For our conditions, the pressure broadening of the Rb D1 line is 15-65 GHz, which far exceeds the Zeeman and hyperfine splittings. Incident, circularly polarized light with magnetic projection +1 (σ_+ light) can only be absorbed by the $5s_{1/2}$ state with $m_s = -\frac{1}{2}$. This populates the $5p_{1/2}$ state with $m_s = +\frac{1}{2}$ which decays to either sublevel of the ground state. In the absence of buffer-gas collisions the $5p_{1/2}$ state with $m_s = +\frac{1}{2}$ decays to either the $5s_{1/2}$ state with relative decay rates given by the Clebsch-Gordon coefficients, $\frac{2}{3}$ for decay to the $m_s = -\frac{1}{2}$ state and $\frac{1}{3}$ for decay to the $m_s = +\frac{1}{2}$ state. However, in our samples, buffer-gas collisions mix the pstates and the relative decay rates to each sublevel of the ground state are $\frac{1}{2}$. As a result, an average of two circularly polarized photons must be absorbed in order that a

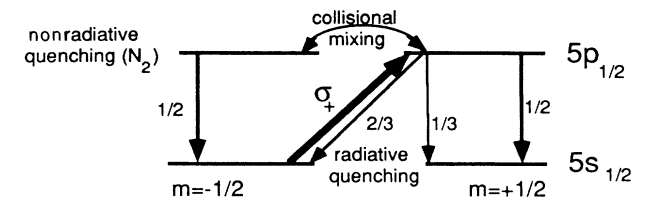


FIG. 3. Demonstration of optical pumping for Rb. The nuclear spin has been neglected and the relevant states are $s_{1/2}$ and $p_{1/2}$. Incident σ_+ light can be absorbed only by the $m=-\frac{1}{2}$ state which is depopulated. Due to buffer-gas collisions the $p_{1/2}$ states are randomized and the probability for decay to either ground state is $\frac{1}{2}$. The Rb resonance linewidth is 15–65 Ghz, much greater than the hyperfine and Zeeman splittings.

single unit of angular momentum is transferred to the atom. Furthermore, the $p_{1/2}$ states decay not only radiatively, but also nonradiatively through collisions with the buffer gas, specifically N_2 , which provides a channel for release of the Rb excitation energy into the vibrational levels of the diatomic molecule. In our cells, the nonradiative rate greatly exceeds the radiative rate. Hrycyshyn and Krausse¹¹ have measured the N_2 -quenching cross section for the $p_{1/2}$ states. Using their value, the branching ratio for radiative decay is given by

$$B_{\gamma} = \frac{3}{3 + P_{N_2}} \tag{1}$$

where P_{N_2} is the N_2 partial pressure at 300 K in torr. We use at least 60 torr of N_2 .

In our model of the optical pumping processes, we assume that the σ_+ light is tuned near the Rb D1 transition and is incident on a cylindrical cell along the cylinder axis (the z axis), and that the light uniformly illuminates the cell. The incident, circularly polarized light provides a flux of photons (photons per unit area per unit frequency per unit time) which is a function of the frequency v and the axial position z: $\Phi(v,z)$. An atom in the state $m_s = +\frac{1}{2}$ cannot absorb a σ_+ photon. Therefore, as the vapor near the front of the cell is optically pumped and the Rb polarization at that position increases with time, the vapor becomes transparent and the light penetrates deeper into the cell. The typical time for the propagation of the polarization along z is 10^{-3} s and $P_{\rm Rb}$ rapidly reaches equilibrium at each position in the cell.

Radiative decay of the $p_{1/2}$ state produces an unpolarized photon which has a shorter, polarization-independent scattering length than the incident circularly polarized photon in the polarized vapor. If it is absorbed by another Rb atom, the unpolarized photon will depolarize the Rb atom and be remitted with branching ratio B_{γ} . If the branching ratio for radiative decay is large enough, a single, incident circularly polarized photon can give rise to multiple-depolarizing scattered photons. This is the phenomenon of radiation trapping which leads to reduced Rb polarization. Radiation trapping will not limit Rb polarization if the probability is sufficiently small for the incident, circularly polarized laser photon to produce an unpolarized photon that is subsequently

absorbed. The probability that this occurs, α , depends on the Rb density and the cell geometry. It is clear, however, that α is proportional to B_{γ} , i.e., inversely proportional to P_{N_2} :

$$\alpha \propto \frac{1}{P_{N_2}}$$
 (2)

The condition that radiation trapping not occur is satisfied when $\alpha \ll 1$. In the model presented here, we assume these conditions and that radiation trapping effects are negligible.

The z dependence of $\Phi(v,z)$ is given by

$$\frac{d\Phi(v,z)}{dz} = -\lambda_{\sigma_+}^{-1}(v,z)\Phi(v,z) . \tag{3}$$

 $\lambda_{\sigma_+}(\nu,z)$ is the absorption length of the incident, right circularly polarized (σ_+) light of frequency ν at the position z:

$$\lambda_{\sigma_{\perp}}^{-1}(v,z) = 2[Rb]\sigma_{s}(v)\rho_{-1/2}(z)$$
 (4)

Here, $\rho_{\pm 1/2}(z)$ is the probability that a Rb atom is in the $m_s = \pm \frac{1}{2}$ state, and $\sigma_s(v)$ is the cross section for scattering of unpolarized light:

$$\sigma_s(v) = \frac{(\Gamma/2)^2}{(v - v_0)^2 + (\Gamma/2)^2} \sigma_0.$$
 (5)

 Γ is the Rb D1 absorption linewidth and the peak cross section σ_0 depends on the total pressure in the cell and is about 10^{-13} cm² for this work.

The probabilities $ho_{\pm 1/2}(z)$ are given by the optical pumping rate equation

$$\left[\frac{\Gamma_{SD}}{2} + \gamma_{opt}(z)\right] \rho_{-1/2}(z) - \frac{\Gamma_{SD}}{2} \rho_{+1/2}(z) + D \nabla_z^2 \rho_{+1/2}(z) = \frac{d}{dt} \rho_{+1/2}(z) .$$
(6)

Here $\gamma_{\text{opt}}(z)$ is the scattering rate of circularly polarized photons per alkali-metal atom in an unpolarized vapor:

$$\gamma_{\text{opt}}(z) = \int \Phi(\nu, z) \sigma_s(\nu) d\nu , \qquad (7)$$

and $\Gamma_{\rm SD}$ is the total rate of destruction of the Rb spin due to collisions. The most important of these are spinnonconserving collisions with other alkali-metal atoms. ^{13,14} Collisions with the N₂ and ³He can be neglected at the densities considered in this work. The last term on the left-hand side of Eq. (6) takes into account diffusion of the populations due to polarization gradients established by boundary conditions at the cell wall and the spatial dependence of $\gamma_{\rm opt}(z)$. D is the diffusion constant for Rb under the conditions in the cell.

We have considered the effects of diffusion in a complete solution to Eq. (6). The boundary condition at the cell wall through which the light is incident is taken to be $\rho_{+1/2} = \rho_{-1/2} = \frac{1}{2}$, i.e., $P_{\rm Rb} = 0$. The polarization grows steeply as a function of z near the cell wall in a length $l = [D/\gamma_{\rm opt}(0)]^{1/2}$ which leads to absorption of the incident light given approximately by $\Delta\gamma_{\rm opt}$

 $=l\sigma_s(\nu)[{\rm Rb}]\gamma_{\rm opt}$. At the buffer-gas densities (D<1) and light intensities of interest $\Delta\gamma_{\rm opt}/\gamma_{\rm opt}(0)$ is less than 1%. We can therefore neglect the effects of diffusion in our present discussion, though we note that consideration of optical pumping at densities much greater than $[{\rm Rb}]=4\times10^{14}$ atoms/cm³, where diffusion effects may not be negligible, is planned to be considered in a separate paper.¹⁵

The Rb spin-destruction rate is therefore taken to be

$$\Gamma_{\rm SD} = \langle \sigma_{\rm SD} v \rangle [\rm Rb] , \qquad (8)$$

where the rate constant $\langle \sigma_{SD} v \rangle = 7.8 \times 10^{-13} \text{ cm}^3 \text{ s}^{-1}$ has been measured by Knize.¹⁴ In the absence of diffusion, the rate equation (6) has the equilibrium solution

$$P_{\rm Rb}(z) = (\rho_{+1/2} - \rho_{-1/2}) = \frac{\gamma_{\rm opt}(z)}{\gamma_{\rm opt}(z) + \Gamma_{\rm SD}}$$
 (9)

Equation (4) can be rewritten

$$\lambda_{\sigma_{+}}^{-1}(\nu,z) = \lambda_{0}^{-1}(\nu) \frac{\Gamma_{SD}}{\gamma_{opt}(z) + \Gamma_{SD}} . \tag{10}$$

Where $\lambda_0^{-1}(v) = [Rb]\sigma_s(v)$ is the inverse of the absorption length for unpolarized light in an unpolarized vapor. These equations can be used to determine the z dependence of $\gamma_{\text{opt}}(z)$ and $P_{\text{Rb}}(z)$.

III. CALCULATIONS

The equations presented above can be solved analytically for narrow-band light and numerically for broadband light. We have considered four cases which are distinguished by the spectral profile and detuning of the laser which produces the circularly polarized light. A dye laser can be used in a narrow-band or a broadband configuration with spectral profile represented by a Lorentzian of FWHM much less than 1 or 40 GHz, respectively. We examine both cases and the effect of tuning a narrow-band laser off resonance for the Rb D1 line. Finally, we present results of numerical calculations using the diode laser array spectral profile shown in Fig. 1.

The numerical calculations have been performed by integrating the differential equation (3) with values for $\gamma_{\rm opt}(z)$ [Eq. (7)], and $\lambda_{\sigma_+}^{-1}(\nu,z)$ [Eq. (10)] determined at each z. We can therefore determine $P_{\rm Rb}(z)$ at each position in the cell and calculate the most important quantity, the average of Rb polarization throughout the cell, $\bar{P}_{\rm Rb}$. As an example, we use the Rb D1 absorption linewidth Γ =15 GHz and a Rb density of 4×10^{14} atoms/cm³, which is typical for our applications. We have also assumed σ_0 = 10^{-13} cm² as determined from our measurements. The light is incident on a cylindrical cell of radius 0.5 cm and length 1.5 cm. The cell volume is 1.65 cm³.

A. Analytic solutions

In order to demonstrate the effectiveness of the broadband light sources for Rb polarization, we will first consider narrow-band light, that is, light with a spectral profile much narrower than the absorption linewidth. In this case $\sigma_s(v)$ is essentially constant across the laser spectrum. Thus the integral of Eq. (7) reduces to

$$\gamma_{\text{opt}}(z) = \sigma_s(v) I_{\text{opt}}(z)$$
, (11)

where $I_{\rm opt}(z)$ is the photon intensity (photons per unit area per unit time) at the position z. This has the analytic solution for $\gamma_{\rm opt}(z)$ given by the transcedental equation

$$\gamma_{\text{opt}}(z) = \gamma_{\text{opt}}(0) - \Gamma_{\text{SD}} \left[\frac{z}{\lambda_0(v)} - \ln \frac{\gamma_{\text{opt}}(0)}{\gamma_{\text{opt}}(z)} \right].$$
 (12)

The average polarization in a cell of length L is then given by

$$\overline{P}_{Rb} = \frac{1}{L} \int_0^L P_{Rb}(z) dz = 1 - \frac{\lambda_0(v)}{L} \ln \left[\frac{\gamma_{\text{opt}}(0)}{\gamma_{\text{opt}}(L)} \right]. \tag{13}$$

The detuning of narrow-band optical pumping light therefore has two consequences: the value of $\gamma_{\rm opt}(z)$ and the value of $\lambda_0(\nu)$. As long as $\gamma_{\rm opt}(z) \gg \Gamma_{\rm SD}$, $P_{\rm Rb}(z) \approx 1$ and

$$\frac{d\gamma_{\rm opt}(z)}{dz} \approx -\frac{\Gamma_{\rm SD}}{\lambda_{\rm o}(v)} \ . \tag{14}$$

Thus $\gamma_{\rm opt}(z)$ decreases linearly with z. At positions where $\gamma_{\rm opt}(z)$ has decreased so much that $\Gamma_{\rm SD}$ can no longer be neglected,

$$\frac{d\gamma_{\rm opt}(z)}{dz} \approx -\frac{\gamma_{\rm opt}(z)}{\lambda_{\rm o}(\nu)} \ . \tag{15}$$

That is, $I_{\rm opt}(z)$ and $\gamma_{\rm opt}(z)$ will decrease exponentially with absorption length $\lambda_0(\nu)$.

B. Pumping with on-resonance light

For zero detuning, the absorption length is $\lambda_0(v_0) \approx \frac{1}{40}$ cm at density [Rb]= 4×10^{14} atoms/cm³ and $P_{\rm Rb}$ will rapidly fall to zero beyond the region where $\gamma_{\rm opt}(z) \gg \Gamma_{\rm SD}$. In this case, the target can be considered as two volumes, one in which the alkali-metal polarization is nearly 100% and the other in which it is nearly 0. The volume of 100% polarized Rb ($V_{100\%}$) depends only on the laser power and the Rb density:

$$V_{100\%} = \lambda_0(v) A \frac{\gamma_{\text{opt}}(0)}{\Gamma_{\text{SD}}} = \frac{AI_{\text{total}}}{\Gamma_{\text{SD}}[\text{Rb}]} , \qquad (16)$$

where $AI_{\rm total}$ is the total rate of incident photon absorption by the Rb vapor in the cell and A is the cross sectional area of the cylinder. Equation (16) predicts that 28 mW of laser power will be absorbed by the alkali-metal vapor for full Rb polarization of 1 cm³ at [Rb]= 4×10^{14} atoms/cm³. For a cell of length L and volume V=AL which is greater than $V_{100\%}$, the average polarization in the cell is given by

$$\bar{P}_{Rb} = \frac{V_{100\%}}{V} = \frac{\lambda_0(v)}{L} \frac{\gamma_{\text{opt}}(0)}{\Gamma_{\text{SD}}} = \frac{L_{\text{total}}}{\Gamma_{\text{SD}}[Rb]L} , \quad (17)$$

which agrees with Eq. (13) in the limit of high polariza-

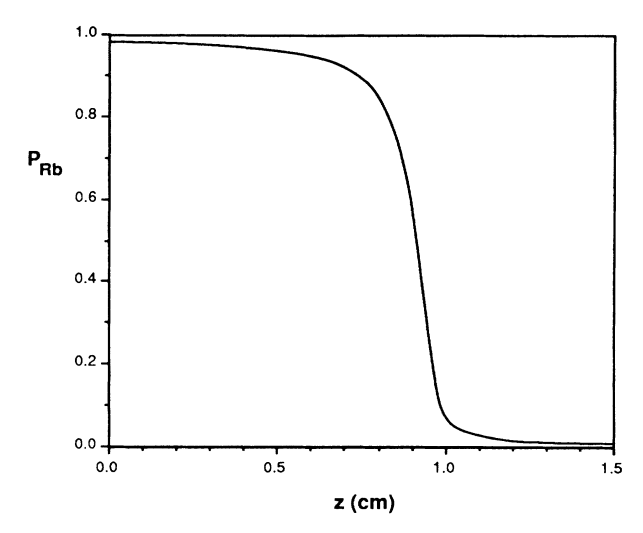


FIG. 4. Results of numerical calculation for narrow-band, on-resonant light. We assume that 25 mW per $\pi/4$ cm² is incident on the Rb. The sharp drop of $P_{\rm Rb}$ separates the cell into two volumes, as described in the text.

tion, i.e., that given by Eq. (14). In fact, Eq. (17) gives the average polarization for light with any spectral profile as long as AI_{total} is defined as the total rate of incident photon absorption by the Rb vapor.

Figure 4 shows the result of a numerical calculation that demonstrates this separation of the cell into two volumes. The laser's spectral width is assumed to be 1 GHz. The cell used for this calculation has $A=\pi/4~{\rm cm}^2$ and $L=1.5~{\rm cm}$. The very sharp drop of $P_{\rm Rb}(z)$ from 1 to 0 indicates the position in the cell where $\Gamma_{\rm SD}$ is no longer much less than $\gamma_{\rm opt}(z)$. The volume in which $P_{\rm Rb}$ is 100% agrees with that predicted by Eq. (16). As we show in Sec. III C, this two-component model is no longer valid if the laser light spectral profile is not confined to a small band centered at the Rb D1 resonance frequency.

C. Pumping with off-resonant light

As the narrow-band light is tuned off the *Rb D1* resonance, $\sigma(\nu)$ decreases and $\lambda_{\sigma_+}(\nu,z)$ increases. $\gamma_{\rm opt}(\nu,z)$ becomes

$$\gamma_{\text{opt}}(\nu, z) = \sigma_0 I_{\text{opt}} \frac{(\Gamma/2)^2}{(\nu - \nu_0)^2 + (\Gamma/2)^2}$$
 (18)

At the front of the cell, $\gamma_{\rm opt}(\nu,z)$ is less than that for the same flux of on-resonance light but the light is more weakly absorbed as it penetrates into the cell. In Figs. 5 and 6 we show the results of our numerical calculation for $\Phi(\nu,z)$ and $P_{\rm Rb}(z)$ as a function of z for incident laser power of 25 mW and detuning $\delta\nu$ of 0, 20, 40, and 60 GHz.

The average $P_{\rm Rb}$ for the cell is shown as a function of detuning $(\delta \nu)$ in Fig. 7 for 25-mW incident laser power and for Rb densities varying from 1.0×10^{14} to 4.3×10^{14} atoms/cm³. In Fig. 7, we take the Rb D1 resonance linewidth to be $\Gamma = 15$ GHz. These curves show that

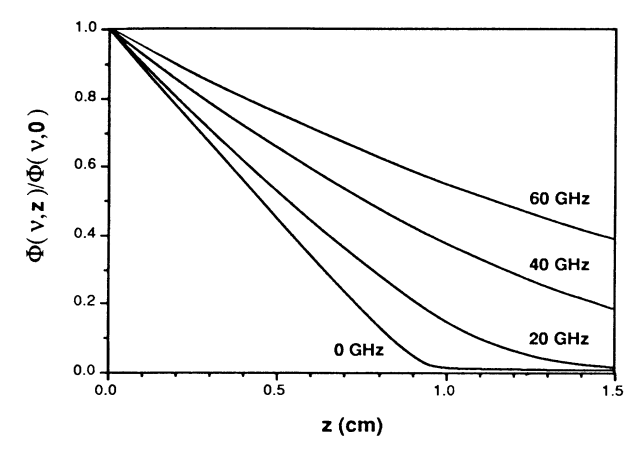


FIG. 5. Photon flux $\Phi(v,z)$ as a function of z for narrow-band light detuned by 0, 20, 40, and 60 GHz. In each case, 25 mW is incident on the vapor.

light detuned by several times Γ can produce high-Rb polarization. Furthermore, the width of the detuning curves of Fig. 7 decreases as [Rb] increases. This is because the region of detuning over which $\bar{P}_{\rm Rb} \approx 1$ given by Eq. (17) increases inversely with $\Gamma_{\rm SD}$.

The dependence on detuning of the average Rb polarization is also strongly dependent on Γ the Rb D1 linewidth. In Fig. 8 we present the detuning curves for [Rb]= 4×10^{14} atoms/cm³ for $\Gamma=15$ and 65 GHz. $\Gamma=65$ GHz is the pressure-broadened linewidth in the 3.7 atmosphere cells we have used in the polarized target applications. Also shown in Fig. 8 is the diode laser array spectral profile of Fig. 1. The curve of Fig. 8 shows that the diode laser array can be very effective for Rb optical pumping in these applications. The results presented in Fig. 8 should also be compared to the measurements described in Sec. IV.

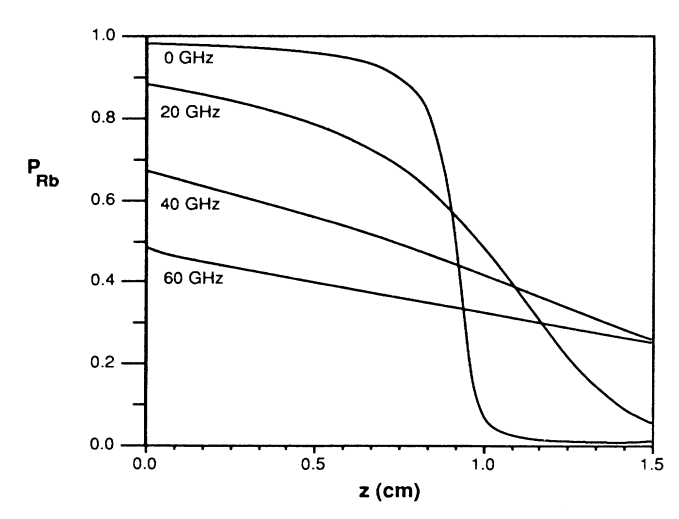


FIG. 6. Rb polarization $P_{\rm Rb}(z)$ as a function of z for narrow-band light detuned by 0, 20, 40, and 60 GHz. In each case, 25 mW is incident on the vapor.

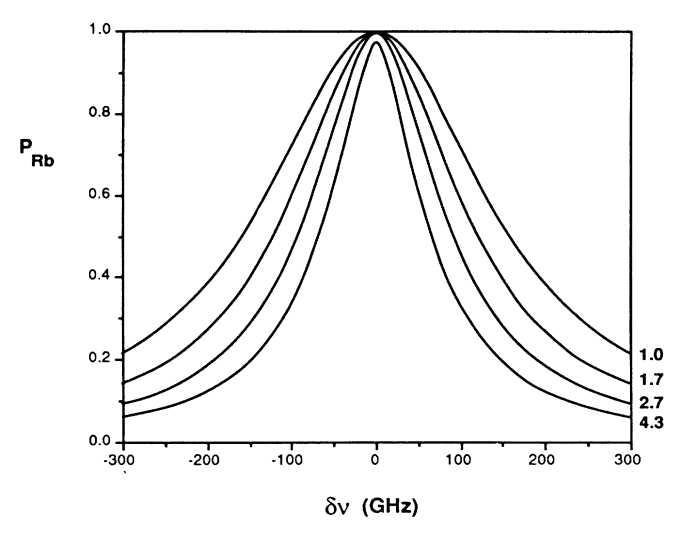


FIG. 7. Calculation of the average Rb polarization in our cell as a function of detuning and [Rb]. [Rb] is shown in units of 10^{14} atoms/cm³. We assume 25 mW per $\pi/4$ cm² is incident on the cell.

D. Optical pumping with broadband dye laser and diode laser array

The dye laser used for most of our previous optical pumping and polarization studies 1,5 is a broadband multimode standing-wave laser (Coherent CR-599) with a three-element birefringent filter. The linewidth has been measured with a scanning monochrometer to be 40 GHz which is used in the calculation described in this section. Thus the absorption length $\lambda_{\sigma_+}(\nu,z)$ varies significantly over the laser spectral profile, and the true effectiveness of the dye laser light is revealed only in the numerical calculations. An example of the diode laser array spectral profile is shown in Fig. 1.

In Fig. 9 we present the results of numerical calcula-

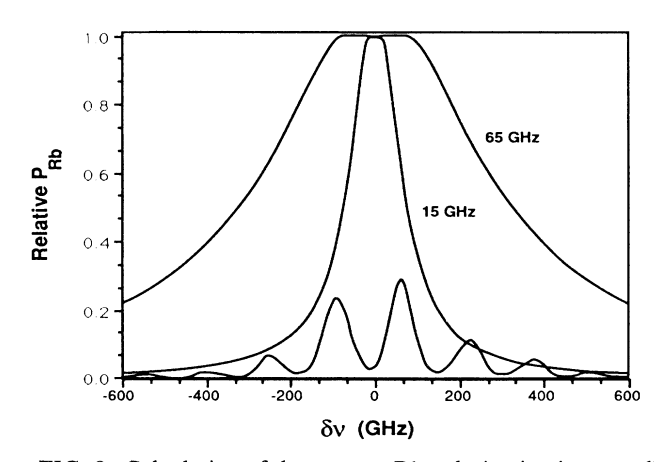


FIG. 8. Calculation of the average Rb polarization in our cell as a function of detuning. The diode-laser-array spectrum (Fig. 1) is superimposed as the dashed curve. We assume that 25 mW per $\pi/4$ cm² is incident on the cell.

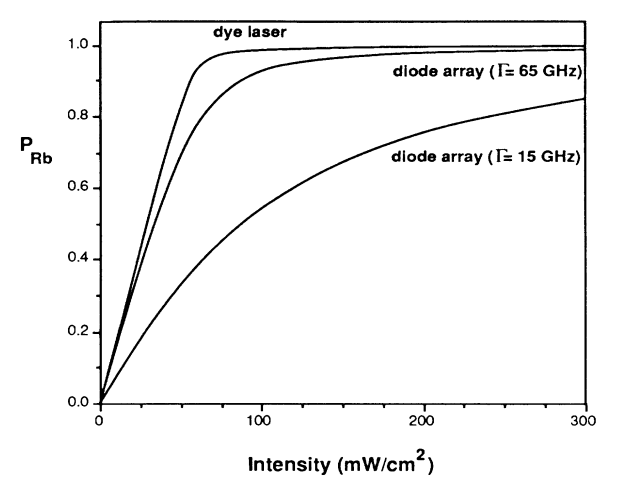


FIG. 9. Calculations of the average Rb polarization in our cell for optical pumping with dye-laser light of 40 Ghz bandwidth and diode-laser light with the spectral profile shown in Fig. 1.

tions of the average Rb polarization in our cell as a function of incident laser power for both the broadband dye laser and the diode laser array. For the dye laser, the spatial profile has been measured and modeled as a Lorentzian which is included in the calculation. The spectrum shown in Fig. 1 is assumed for the output of the diode laser array. The shaping of the diffraction-limited, two-lobed spatial profile of the array generally results in diminished power. We have made measurements with 30–300 mW of power from the dye laser and the two diode laser arrays, of nominal power 100 and 500 mW. The nearly identical performance expected, under these conditions, from the dye laser and diode laser array is shown in Fig. 9 and confirmed by the measurement described below.

IV. MEASUREMENTS OF Rb AND ³He POLARIZATION

In order to confirm the results of the numerical calculations of Rb polarizations, we have measured 3 He polarization rates which can be used to determine the average $P_{\rm Rb}$. The rate of polarization of 3 He by spin exchange with optically pumped Rb is 1

$$\frac{dP_{^{3}\text{He}}}{dt} = \overline{P}_{\text{Rb}} \gamma_{\text{SE}} e^{-(\gamma_{\text{SE}} + \Gamma)t} . \tag{19}$$

 $\gamma_{\rm SE}=k_{\rm SE}[{\rm Rb}]$ is the spin-exchange rate where the velocity averaged rate constant $k_{\rm SE}=\langle\sigma_{\rm SE}v\rangle=1.2\times10^{-19}~{\rm cm}^3{\rm s}^{-1}$ has been measured. For ${\rm [Rb]}=4\times10^{14}$ atoms/cm³, $\gamma_{\rm SE}=1/(6~{\rm h})$. Γ is the total He spin-relaxation rate which depends on cell wall interactions and magnetic field inhomogeneity. For our work, Γ varies from $1/(2~{\rm h})$ for cells made of boro-silicate (Pyrex) glass to less than $1/(200~{\rm h})$ for cells made of aluminosilicate (e.g., Corning 1720) glass. For short times such that $(\gamma_{\rm SE}+\Gamma)t\ll1$, Eq. (19) reduces to

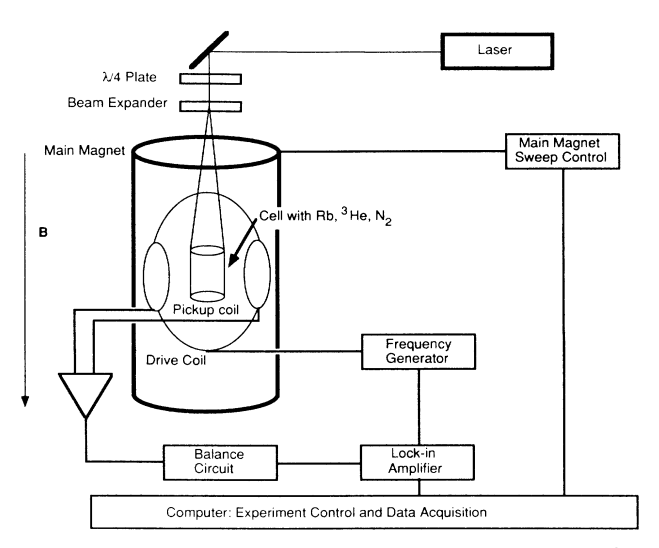


FIG. 10. Apparatus used to optically pump Rb, polarize ³He, and measure the ³He polarization. The apparatus is described in the text.

$$\frac{dP_{^{3}\text{He}}}{dt} = \bar{P}_{Rb}\gamma_{SE} \ . \tag{20}$$

We therefore determine the average of P_{Rb} in the cell by measuring the ${}^{3}\text{He}$ polarization rate.

The apparatus used for these ³He polarization rate measurements is similar to that used for previous investigations^{1,2,5} and is described only briefly in this paper. The apparatus is illustrated in Fig. 10. It consists of the laser and optics, the coils to produce the static magnetic field **B**, and the adiabatic-fast-passage polarimeter to measure the ³He polarization.

The cells are prepared by cleaning with water and methanol and evacuating to $\approx 10^{-7}$ torr while baking at 400 °C for at least 8 h. The alkali metal is then introduced into the cells by distillation with a flame. 60-325 torr of N_2 and about 600 torr of 3 He are mixed in the cell.

³He polarization is measured with a NMR adiabatic-fast-passage (AFP) polarimeter also illustrated in Fig. 10. The ³He nuclei are polarized along the z axis. An oscillating magnetic field $(2\mathbf{B}_x\cos\omega t)$ is applied, typically 10-mG amplitude at 120 kHz. As the static field \mathbf{B}_z is swept from below resonance to above and back down the nuclear magnetization follows the net field in the rotating frame; $\mathbf{B}_{\rm rot} = (B_z - \omega/\gamma)\hat{\mathbf{z}} + B_x\hat{\mathbf{x}}$, i.e., it rotates from parallel to opposite \mathbf{B}_z and back. The sweep rate dB_z/dt is sufficiently slow to satisfy the adiabatic condition. During the process of rotating, the magnetization precesses in the laboratory frame at the rate $\omega = 2\pi\gamma |\mathbf{B}_z|$. The precessing magnetization induces a voltage in the pickup coils oriented along the y axis:

$$V_0 = \omega \Phi NQ , \qquad (21)$$

where Φ is the flux through the pickup coil's N turns and the coil forms part of a tuned circuit with quality factor Q. Φ is proportional to the magnetization [${}^{3}\text{He}$] $P_{3}\mu_{3}$. The ${}^{3}\text{He}$ polarization is directly calibrated with signals

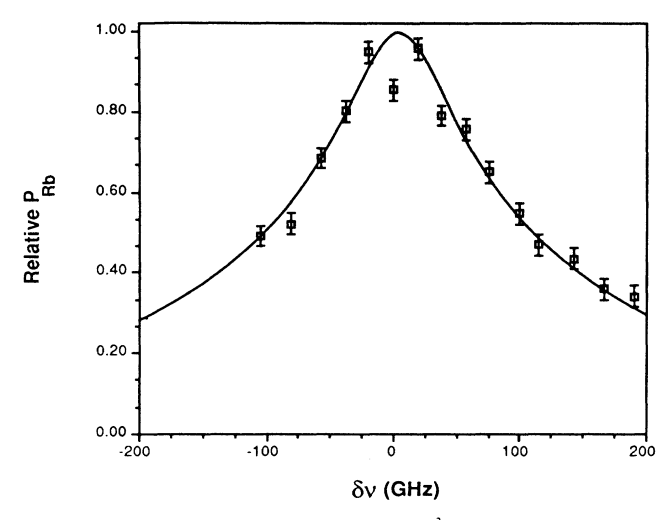


FIG. 11. Results of measurement of 3 He polarization rates and therefore the relative $P_{\rm Rb}$ as a function of detuning from the Rb D1 resonance line center. Also shown as the solid line is the result of the calculation presented in Fig. 8.

produced by protons in distilled H_2O which are polarized due to thermal equilibrium in the applied magnetic field. Any change in the response of the pickup coils due to temperature, inductance, etc. is monitored with a single-turn coil wound parallel to the pickup coil and driven at the drive coil frequency. The AFP technique is particularly useful because it is nondestructive, i.e., the polarization can be probed and returned to its initial condition with less than 2% loss of polarization.

In Fig. 11 we show the measured relative ³He polarization rate as a function of detuning of the dye laser from the Rb resonance. For these measurements, we used a single thin étalon in the dye-laser cavity to produce essentially a laser with linewidth less than 3 GHz. The conditions of the measurement are Rb D1 resonance linewidth $\Gamma = 15 \text{ GHz}$, [Rb] = 1.7×10¹⁴ atoms/cm³, and $P_{N_2} = 325$ torr at 300 K. We note the small drop of P_{Rb} . This dip may be due to the onset of radiation trapping which is more apparent at higher [Rb] and will be discussed in a separate paper. 15 Also shown in Fig. 11 is the result of a calculation of P_{Rb} for the same conditions, which is scaled in order to compare with the measurement of the ³He polarization rates. The data away from zero detuning are normalized to this calculation in order to show that with the exception of the $\delta v = 0$ data point, the agreement of the calculated shape and measurement is quite good. We have compared the ³He polarization

rates produced with both the dye-laser and diode-laser arrays at powers of 30 and 300 mW. The results are comparable and in agreement with the calculation presented in Fig. 9.

V. SUMMARY

We have presented numerical calculations and measurements which demonstrate the effectiveness for high-density Rb optical pumping and ³He polarization of both a multimode dye laser and commercially produced diode laser arrays. Due to the high total pressure in our cells, the Rb D1 resonance linewidth is pressure broadened to 18 Ghz per atmosphere of total pressure. We have produced cells with pressure up to 3.7 atm and 65 Ghz linewidth. Circularly polarized light more than 100 Ghz off resonance can be effective for optical pumping. It is therefore possible to make use of broadband lasers including diode laser arrays. Our conclusions are summarized in the following.

- (i) Optical pumping with on-resonance light from a narrow-band laser (where the Rb D1 absorption linewidth is much greater than the laser linewidth) can be understood with the two-component model where the average Rb polarization is given by Eq. (17).
- (ii) Off-resonant light is effective for optical pumping under our conditions of a broad absorption line and high-Rb density. The detuning profiles shown in Figs. 7 and 8 depend on the cell geometry as well as the Rb D1 linewidth and Rb density.
- (iii) The diode laser array can be as effective for Rb optical pumping and ³He polarization as our dye laser.

We are using 500-mW or 1-W diode laser arrays for our polarized target development and precision frequency shift measurements. More than one laser will make possible larger volume and/or greater ³He polarization rates. This laser power will be available at an expense far less than that for the dye-laser system.

ACKNOWLEDGMENTS

The authors wish to thank W. Happer and R. Loveman for many useful suggestions and criticisms. We gratefully acknowledge the donation by Spectra Diode Laboratories, San Jose, California, of diode laser arrays used in this research. This material is based upon work supported by a National Institute of Standards and Technology Precision Measurement grant, a grant from the Research Corporation, and the National Science Foundation under Grants No. Phy-8605081 and No. Phy-8604510. T. E. C. acknowledges the support of the Alfred P. Sloan Foundation.

¹T. E. Chupp, M. E. Wagshul, K. P. Coulter, A. B. McDonald, and W. Happer, Phys. Rev. C 36, 2224 (1987).

²K. P. Coulter, A. B. McDonald, W. Happer, T. E. Chupp, and M. E. Wagshul, Nucl. Instrum. Methods A 270, 90 (1988).

³T. E. Chupp et al., Bull. Am. Phys. Soc. **33**, 905 (1988).

⁴T. E. Chupp, E. R. Otieza, J. M. Richardson, and T. R. White, Phys. Rev. A 38, 3998 (1988).

⁵T. E. Chupp and K. P. Coulter, Phys. Rev. Lett. **55**, 1074 (1985).

⁶M. A. Bouchiat, T. R. Carver, and C. M. Varnum, Phys. Rev.

Lett. 5, 373 (1960).

- ⁷R. L. Gamblin and T. R. Carver, Phys. Rev. A **138**, 964 (1965).
- ⁸H. Hemmati, Appl. Phys. Lett. **51**, 224 (1987).
- ⁹L. Goldberg et al., Appl. Phys. Lett. **46**, 236 (1985).
- ¹⁰J. P. Hohimer, A. Owyoung, and G. R. Hadley, Appl. Phys. Lett. 47, 1244 (1985).
- ¹¹E. S. Hrycyshyn and L. Krausse, Can. J. Phys. 48, 2761 (1970).
- ¹²N. D. Bhaskar, M. Hou, B. Suleman, and W. Happer, Phys.
- Rev. Lett. 43, 519 (1979).
- ¹³N. D. Bhaskar, J. Pietras, J. Comparo, W. Happer, and J. Miron, Phys. Rev. Lett. **44**, 930 (1980).
- ¹⁴R. Knize and W. Happer, Bull. Am. Phys. Soc. 30, 866 (1985);R. Knize (private communication).
- 15T. E. Chupp, M. E. Wagshul, and R. A. Loveman (unpublished).